Electronic Supplementary Material (ESI) for Nanoscale.

Supporting material for: Controlling Photon Antibunching from 1D Emitters using Optical Antennas

Lucas Lange, Frank Schäfer, Alexander Biewald, Richard Ciesielski, and Achim Hartschuh

Department of Chemistry and Center for NanoScience (CeNS),

*LMU Munich, Butenandtstr. 5-13, 81377 Munich, Germany**

1. NEAR-FIELD OPTICAL MICROSCOPE SETUP

The setup for antenna-enhanced experiments combines an inverted confocal microscope with shear-force based tuning fork feedback for operating a sharp gold tip in close distance to the sample. A tunable picosecond laser (repetition rate 40 MHz, pulse duration below 1 ps) is used to provide resonant excitation at 570 nm matching the E_{22} transition in semiconducting (6,5) SWCNTs [1]. Importantly, the laser pulse duration is substantially shorter than the exciton lifetime of around 10-50 ps [2] to avoid multiple sequential excitations within a pulse. Before entering the microscope, the laser mode was converted into a radially polarized donut mode to generate a strong longitudinal field component in the focus of the high numerical aperture objective (NA=1.49) [3]. The PL of SWCNTs deposited on microscope glass cover slides was detected at the first excitonic resonance around 980 nm after spectral filtering using a Hanbury-Brown-Twiss configuration in combination with two sensitive avalanche photodiodes (APDs).

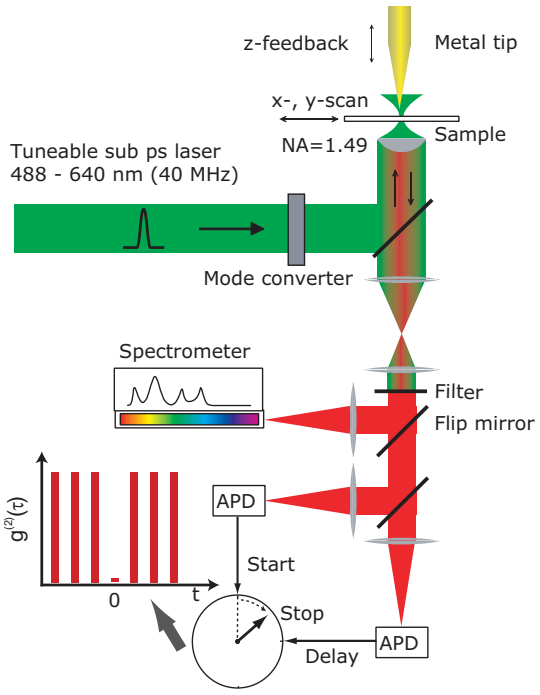

FIG. S1: Schematic illustrating the tip-enhanced near-field optical microscope setup.

2. CARBON NANOTUBE SYNTHESIS AND SURFACTANT DISPERSION

CoMoCat SWCNTs (Product No. 704148, SG65) were purchased from Sigma-Aldrich. Initial 1 mg/ml suspensions of this starting materials were prepared as aqueous 1% sodium deoxycholate (DOC, BioXtra, Sigma-Aldrich) using 8 min of tip sonication (Bandelin Sonoplus HD2200/UW 2200, 17-18% power level) under ice cooling. A two-step aqueous two-phase separation [4] was used to enrich the (6,5) chirality, using polyethylene glycol (PEG-6000, BioXtra, Alfa Aesar), Dextran-70 (Tokyo Chemical Industry), sodium cholate (SC, 99 %, Sigma-Aldrich), sodium dodecyl sulfate (SDS, BioXtra, Sigma-Aldrich), sodium chloride (BioXtra, Sigma-Aldrich) and nanopure water. The ultracentrifugation (Eppendorf 5430) was operated using Amicon filter tubes (100kDa, PLHK Ultracel, Millipore).

In addition to (6,5) enriched SWCNT in DOC and SDS surfactant dispersion, we also used DNA-wrapped SWCNTs as samples using the purification steps according to Ao et al. [5]. HPLC-purified Oligonucleotides were purchased from Metabion International AG (Planegg, Germany), consisting of the Sequence CCG CCG CC, having showed a 11% yield for (6,5) chiralities [5]. The DNA-wrapped SWCNTs we obtained were not treated with SDS or DOC.

3. PL EMISSION STATISTICS OF SWCNTS WITHOUT OPTICAL ANTENNA

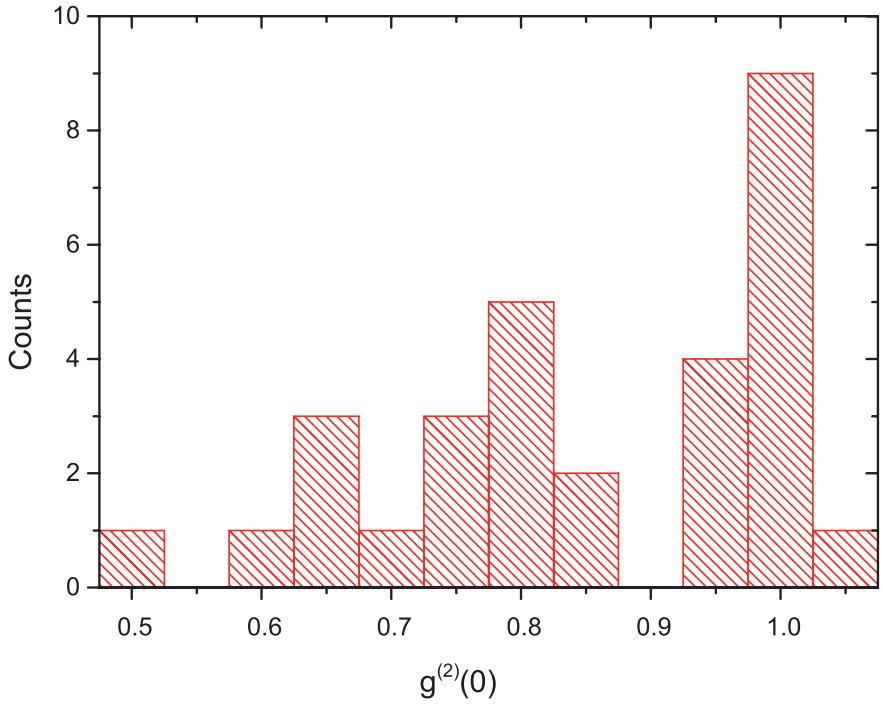

FIG. S2: Histogram of the second order intensity correlation function at t = 0 ($g^{(2)}(0)$) from single (6,5) nanotubes observed without optical antenna.

Figure S2) shows the histogram of the second order intensity correlation function at t = 0 ($g^{(2)}(0)$) obtained for single (6,5) SWCNTs on glass using confocal microscopy. The distribution of $g^{(2)}(0)$ is centered at 0.8 and ranges from 0.5 to 1.0. The observed values are in general agreement with reports in literature and reflect the interplay between exciton diffusion, localization and exciton-exciton annihilation, which is expected to vary because of the heterogeneities in the nanotubes' environment, different nanotube length and local defect densities [6–8].

4. PL EMISSION OF SWCNTS WITH OPTICAL ANTENNA: ADDITIONAL DATA

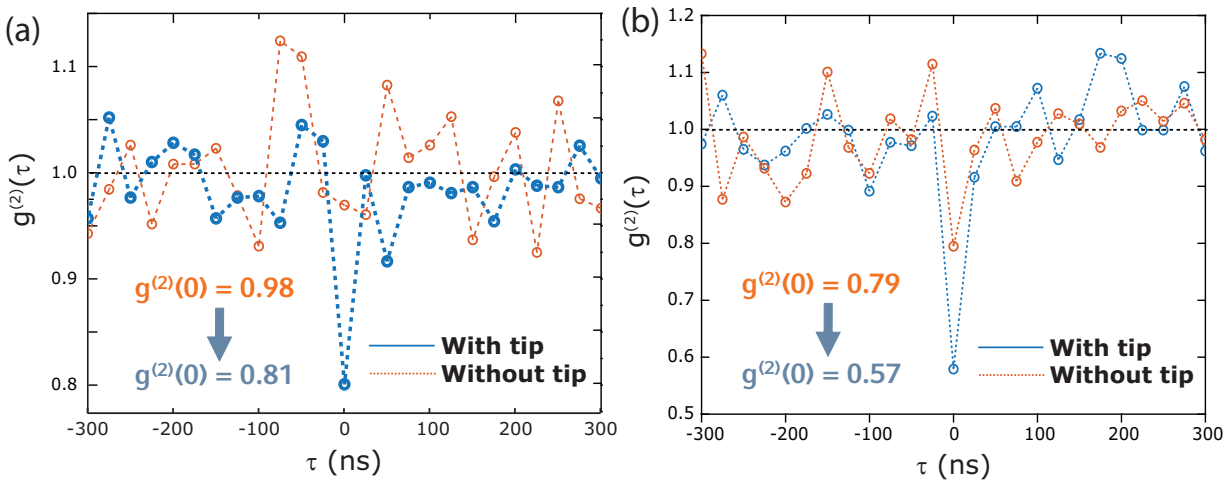

FIG. S3: Antenna-controlled antibunching: Normalized second order correlation function $g^{(2)}(\tau)$ of the PL from two different single (6,5) SWCNTs with and without tip antenna.

Figure S3(a) and (b) show the normalized second order correlation function $g^{(2)}(\tau)$ detected for two different (6,5) single-walled carbon nanotube on glass with and without optical antenna. In both cases, the antenna reduces $g^{(2)}(0)$ by about 0.2. Whereas (6,5) SWCNTs in DOC and SDS surfactants exhibited lower $g^{(2)}(0)$ as compared to DNA-wrapped (6,5) SWCNTs in general, the antenna-controlled reduction of $g^{(2)}(0)$ was found to be same.

5. MONTE-CARLO SIMULATIONS: ADDITIONAL DATA AND DISCUSSION

A schematic of the Monte-Carlo simulation is shown in Fig. 2 of the main manuscript. The 281.6 nm long 1D nanostructure is discretized into 256 steps of 1.1 nm, corresponding to the approximate exciton Bohr radius of SWCNTs [9]. An initial, randomly distributed population of excitons with a density proportional to the light intensity at the nanotube is created. The Monte-Carlo code simulates a random walk of the excitons along the nanotube, with a set probability of radiative or non-radiative decay for each time step. The probability of radiative decay is locally modulated by the near-field intensity of the tip, scaling with the field enhancement factor f. For simplicity, we neglect the vectorial character of the fields and treat f as a scalar $f = E/E_0$ [3]. If an exciton reaches the end of the nanotube, it is quenched. If two excitons occupy the same position, they annihilate resulting in one remaining exciton. The size of the time steps is calculated from the diffusion length and the lifetime, such that one time step corresponds to the travel time between two lattice positions. For a given set of parameters, the simulation is executed about 10^{12} times in a distributed fashion, recording the number of radiative decay events in each run from which the value of $g^{(2)}(0)$ is calculated [8].

In Fig. 3 of the main manuscript, we illustrate the influence of field enhancement f, near-field confinement d, initial exciton density N and diffusion length L_D on the degree of antibunching. Here, we discuss the influence of three more parameters on the results of the Monte-Carlo simulations: the photoluminescence quantum yield QY, the presence of a shallow energy minimum, and the influence of radiative rate enhancement.

Figure S4(a) provides simulated data for varying quantum yield of the nanotube. The PL quantum yield of a nanotube without the interaction with a nano-tip is defined as the ratio of radiative and the sum of all decay rates:

$$QY = \frac{k_{radiative}}{k_{radiative} + k_{non-radiative}}, \tag{1}$$

and the total lifetime τ is given by:

$$\frac{1}{\tau} = k_{radiative} + k_{non-radiative}. \tag{2}$$

Figure S4(a) shows the hypothetical case that only the quantum yield changes, but not the overall lifetime. Apparently, a lower quantum yield is beneficial for the degree of antibunching if a tip is present. This can be understood as an effect of residual excitons created in

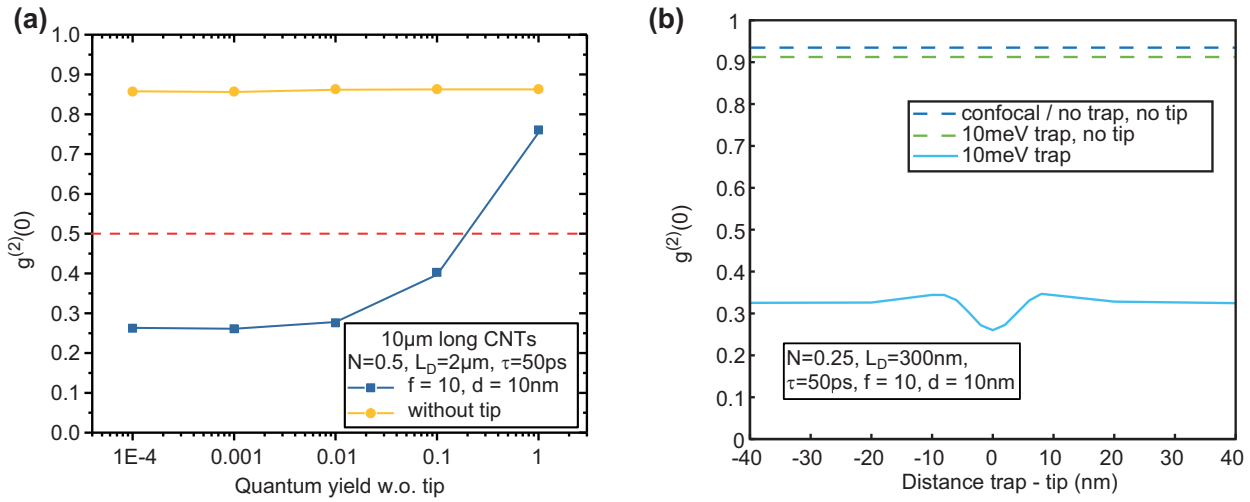

FIG. S4: (a) Influence of the nanotube's PL quantum yield QY on $g^{(2)}(0)$. (b) The presence of a shallow energy minimum that localizes excitons at one point will further decrease $g^{(2)}(0)$ if it is located below the nano-tip antenna.

the confocal spot, whose number is not controlled by the antenna effect. If the quantum yield is low, those uncontrolled excitons have a very low probability to decay into a photon, so in return the emission will mostly originate from the near-field area, where the radiative rate is enhanced. For a high quantum yield, it becomes much more likely that excitons from outside the near-field area decay into a photon, which disturbs the envisaged photon statistic. Adversely, low quantum yield also means low emission yield.

Shallow energy minima can lead to partial exciton localization [10], which provides an additional path to photon-antibunching. Figure S4(b) shows a simulation where an energy minimum of 10 meV depth and 5 nm width is implemented as a dip in the energy landscape $E(x)$:

$$E(x) = -10\,\mathrm{meV} \cdot \exp(-4 \cdot \log 2 \cdot x^2/(5\,\mathrm{nm})^2). \tag{3}$$

Around the energy minimum, the probability for the exciton to go to the right or to the left position is modulated by the Boltzmann distribution at a thermal energy of 25 meV (room temperature):

$$P_{right}(x) = \frac{1}{1 + \exp\left[\left(E(x+\Delta x) - E(x-\Delta x)\right)/25\,\mathrm{meV}\right]}, \quad P_{left}(x) = 1 - P_{right}(x). \tag{4}$$

Δx is the distance between two numerical lattice positions. In the confocal case, the existence of a shallow energy minimum lowers $g^{(2)}(0)$, although not much for the present

parameters (Fig. S4b). If an antenna is present and it is positioned at the location of the energy minimum, the degree of antibunching is significantly increased. This shows, that the combination of exciton localization and the antenna effect has a good potential for future applications.

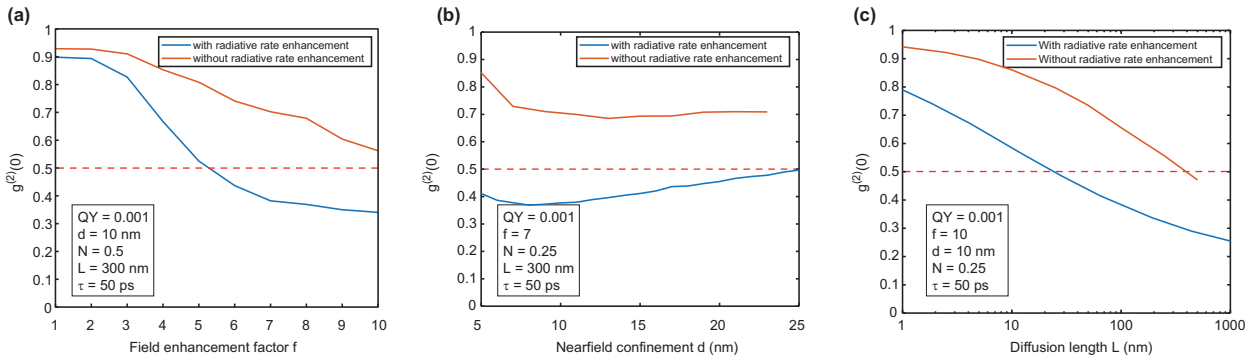

FIG. S5: Influence of radiative rate enhancement on the value of $g^{(2)}(0)$. In all cases, $g^{(2)}(0)$ is reduced significantly if radiative rate enhancement is present: (a) for varying field enhancement factor f, (b) for varying field confinement d, (c) for varying exciton diffusion length L_D.

The radiative rate enhancement in the near-field of a nano-antenna in the Monte-Carlo simulations is described through a locally modulated value of the radiative rate:

$$k_{radiative}(x) = \frac{QY}{\tau} \cdot (1 + f^2 \cdot \exp(-4 \cdot \log(2) \cdot x^2/d^2)). \tag{5}$$

It is possible that the value of f is different for excitation and detection since it usually depends on the wavelength. A large energy shift between excitation and detection can lead to the situation that only one of the two cases are resonant with the antenna. Figure S5 compares the double resonant situation with the situation where only the excitation is resonant with the antenna. For detection $f = 1$ is assumed, which results in a zero radiative rate enhancement at the antenna. We observe that the general trends with field enhancement factor, near-field confinement and diffusion length are reproduced as in the main text, but all cases are less pronounced. Radiative rate enhancement results in $g^{(2)}(0)$ that is on average 0.2 lower than in the case where only the excitation is resonant with the antenna. As discussed earlier, a lower quantum yield will further enhance this effect, but at the expense of a lower total photon output.

* Electronic address: achim.hartschuh@lmu.de

[1] Bachilo, S. M. *et al.* Structure-assigned optical spectra of single-walled carbon nanotubes. *Science* **298**, 2361–2366 (2002).

[2] Gokus, T. *et al.* Mono- and biexponential luminescence decays of individual single-walled carbon nanotubes. *J. Phys. Chem. C* **114**, 14025–14028 (2010).

[3] Mauser, N. & Hartschuh, A. Tip-enhanced near-field optical microscopy. *Chem. Soc. Rev.* **42**, 1248 (2014).

[4] Subbaiyan, N. K. *et al.* Role of Surfactants and Salt in Aqueous Two-Phase Separation of Carbon Nanotubes toward Simple Chirality Isolation. *ACS Nano* **8**, 1619 (2014).

[5] Ao, G., Khripin, C. Y. & Zheng, M. DNA-Controlled Partition of Carbon Nanotubes in Polymer Aqueous Two-Phase Systems. *J. Am. Chem. Soc.* **136**, 10383 (2014).

[6] Endo, T., Ishi-Hayase, J. & Maki, H. Photon antibunching in single-walled carbon nanotubes at telecommunication wavelengths and room temperature. *Appl. Phys. Lett.* **106**, 113106 (2015).

[7] Ma, X. *et al.* Influences of Exciton Diffusion and Exciton-Exciton Annihilation on Photon Emission Statistics of Carbon Nanotubes. *Phys. Rev. Lett.* **115**, 017401 (2015).

[8] Ishii, A., Uda, T. & Kato, Y. K. Room-Temperature Single-Photon Emission from Micrometer-Long Air-Suspended Carbon Nanotubes. *Phys. Rev. Appl.* **8**, 054039 (2017).

[9] Capaz, R. B., Spataru, C. D., S., I.-B. & Louie, S. G. Diameter and chirality dependence of exciton properties in carbon nanotubes. *Phys. Rev. B* **74**, 121401(R) (2006).

[10] Georgi, C., Green, A. A., Hersam, M. C. & Hartschuh, A. Probing exciton propagation and quenching in carbon nanotubes with near-field optical microscopy. *ACS Nano* **4**, 5914 (2010).